Stability and Resistance of Nickel Catalysts for Hydrodeoxygenation: Carbon deposition and effects of Sulfur, Potassium, and Chlorine in the Feed

Peter M. Mortensen,[a‡] Diego Gardini,[b] Hudson W. P. de Carvalho,[c] Christian D. Damsgaard,[b,d] Jan-Dierk Grunwaldt,[c] Peter A. Jensen,[a] Jakob B. Wagner,[b] and Anker D. Jensen*[a]

[a] *Department of Chemical and Biochemical Engineering, Technical University of Denmark, Søltofts Plads, Building 229, DK-2800 Lyngby, Denmark. Fax: +45 4588 2258 Tel.: +45 4525 2841. E-mail address: aj@kt.dtu.dk.*
[b] *Center for Electron Nanoscopy, Technical University of Denmark, Fysikvej, Building 307, DK-2800 Lyngby, Denmark*
[c] *Institute for Chemical Technology and Polymer Chemistry, Karlsruhe Institute of Technology (KIT), Engesserstrasse 20, D-79131 Karlsruhe, Germany*
[d] *CINF, Department of Physics, Technical University of Denmark, Fysikvej, Building 307, DK-2800 Lyngby, Denmark*

S-1 Reduction Temperature of Ni/ZrO_2

To evaluate the required reduction temperature, the reduction of the calcined NiO/ZrO_2 was monitored by in-situ XAS, Figure 1(a) presents the evolution of the Ni-K near edge region as function of the temperature. The decrease in the absorption threshold intensity during the activation step show that Ni was being reduced. Furthermore, all spectra shown in Figure 1(a) are superposed at the same isosbestic points indicating that conversion of calcined Ni species to the reduced Ni phase took place in a single step. The fraction of oxidized and reduced phase was estimated by linear combination analysis and is presented in Figure 1(b). The reduction rate strongly increased from 264 °C and was completed at 450 °C. Thus, in all experiments a reduction temperature of 500 °C was used to ensure complete reduction of the catalysts.

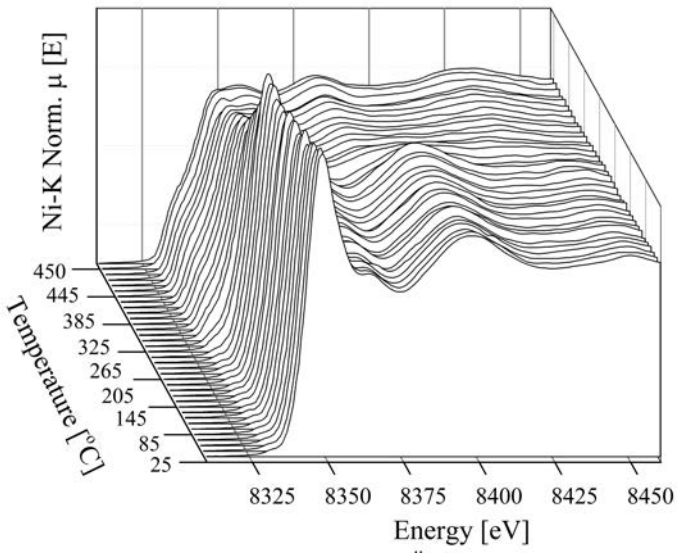

(a) Ni-K X-ray absorption near edge spectra

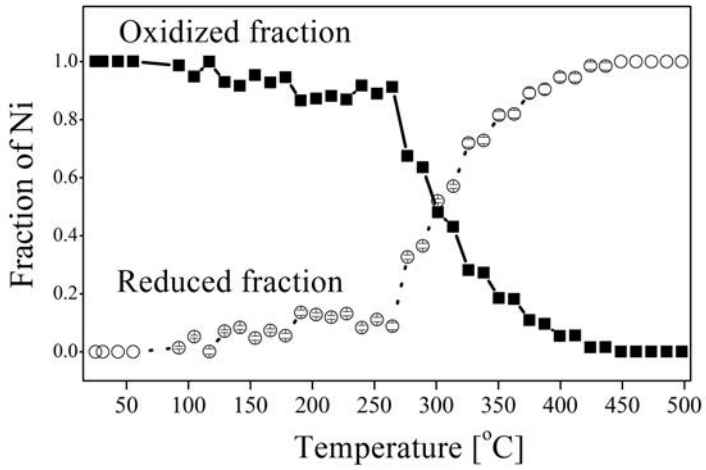

(b) Fraction of oxidized and reduced Ni

Figure S-1: Ni-K X-ray absorption near edge spectra recorded as function of the temperature during the reduction of the catalyst (a) and linear combination results estimating the fraction of oxidized and reduced Ni phases during the reduction of the catalyst (b).

S-2 Transport Limitations

To evaluate the effect of the external diffusion, Mears' criterion for external diffusion was used. This states that the external diffusion limitations can be neglected if [1]:

$$C_M = \frac{r'(obs) \cdot \rho_b \cdot d_p \cdot n}{2 \cdot k_c \cdot C_{Ab}} < 0.15 \tag{S-1}$$

Here r' is a measured reaction rate, ρ_b is the bulk density of the catalyst bed (found as 950 kg/m^3), d_p is the diameter of the catalyst particles, n is the reaction order, k_c is the mass transfer coefficient, and C_{Ab} is the concentration of reactant A in the bulk.

Mears' criterion is an evaluation of the external diffusion of one compound. As hydrogenation of guaiacol is the fastest reaction in the present system, this reaction will be evaluated and therefore the diffusion of this in 1-octanol.

The reaction rate is evaluated on the basis of the kinetic model developed for the system and the reaction rate in the inlet to the system is used:

$$r_1 = k_1' \cdot C_{0,\text{Guaiacol}} \cdot (1 - X_1) \tag{S-2}$$

$$= 500ml/(kg \cdot min) \cdot 900mol/m^3 \cdot (1 - 0) \tag{S-3}$$

$$= 7.5 \cdot 10^{-3} mol/(kg \cdot s) \tag{S-4}$$

The particle diameter was controlled by sieving the catalyst, obtaining a particle size in the range from 300 μm to 600 μm. In order to consider the worst case scenario, the largest particle diameter was used in the calculations.

The reaction order was assumed to be 1.

D_{AB} was estimated from the Wilke-Chang method [2]:

$$D_{AB} = 7.4 \cdot 10^{-8} \cdot \frac{\sqrt{\psi_B \cdot M_B} \cdot T}{\mu \cdot \tilde{V_A}^{0.6}} \tag{S-5}$$

Here ψ_B is an association parameter assumed to be 1 for 1-octanol [3], M_B the molar mass of 1-octanol (130.23 g/mol), T the temperature in Kelvin, μ the viscosity of the mixture in cP (0.65 cP for 1-Octanol [4]), and $\tilde{V_A}$ is the molar volume of guaiacol in cm^3/mol (111.6 cm^3/mol). In this way the diffusion coefficient for guaiacol in 1-octanol can be found as $4.01 \cdot 10^{-9}$ m^2/s. This is needed to calculate k_c, which will be done from the correlation between the Reynolds number (Re), the Schmidt number (Sc) and the Sherwood number (Sh). The estimated Reynolds and Schmidt numbers are:

$$Re = \frac{\frac{F}{A} \cdot d_p \cdot \rho_l}{\mu} \tag{S-6}$$

$$= \frac{\frac{0.2ml/min}{5 \cdot 10^{-5} m^2} \cdot 0.6mm \cdot 0.824g/ml}{0.65cP} = 0.13 \tag{S-7}$$

$$Sc = \frac{\mu}{\rho_l \cdot D_{AB}} \tag{S-8}$$

$$= \frac{0.65cP}{0.824g/ml \cdot 4.01 \cdot 10^{-9} m^2/s} = 197 \tag{S-9}$$

Here F is the flow, A the cross section area, and ρ_l the density of the liquid. These can be used to calculate the Sherwood number (Sh) [1]:

$$Sh = \left(\frac{0.765}{Re^{0.82}} + \frac{0.365}{Re^{0.386}} \right) \frac{Sc^{1/3} \cdot Re}{1 - \phi_b} \tag{S-10}$$

$$= \left(\frac{0.765}{0.13^{0.82}} + \frac{0.365}{0.13^{0.386}} \right) \frac{197^{1/3} \cdot 1.45}{1 - 0.4} = 8.22 \tag{S-11}$$

Here ϕ_b is the porosity of the bed, which was assumed to be 0.4.

The mass transfer coefficient is obtained from the Sherwood number:

$$k_c = \frac{Sh \cdot D_{AB}}{d_p} \tag{S-12}$$

$$= \frac{8.22 \cdot 4.01 \cdot 10^{-9} m^2/s}{0.6mm} = 5.50 \cdot 10^{-5} m/s \tag{S-13}$$

From this, Mears can now be found to be 0.04, which is significantly lower than 0.15 and thereby indicating that the reaction is not limited by external diffusion.

Based on the previous results of no external diffusion limitation the Weisz-Prater criteria can be used in the estimation of internal diffusion limitations [1]:

$$C_{wp} = \frac{r'(obs) \cdot \rho_c \cdot \left(\frac{d_p}{2}\right)^2}{D_e \cdot C_{As}} \tag{S-14}$$

Here D_e is the effective diffusion coefficient, and C_{As} is the concentration of the investigated compound at the surface of the catalyst.

$r'(obs)$ is determined analogously to what was done in Eq. S-2, and d_p is the same catalyst particle diameter as discussed above. C_{As} can be assumed equal to the concentration in the bulk, because it was concluded that there was no external diffusion limitation.

The effective diffusion coefficient is estimated as:

$$D_e = \frac{\phi_c \cdot \vartheta_c}{\tau_c} \cdot \frac{1}{\frac{1}{D_K} + \frac{1}{D_{AB}}} \tag{S-15}$$

Here ϕ_c is the porosity of the catalyst, ϑ_c is the constriction factor, and τ_c is the tortuosity.

The Knudsen diffusivity, D_K, is given by [5]:

$$D_K = 9700 \cdot a \cdot \left(\frac{T}{M_A}\right)^{1/2} \tag{S-16}$$

$$= 9700 \cdot 2 \cdot 10^{-6} cm \cdot \left(\frac{523K}{124.14 g/mol}\right)^{1/2} \tag{S-17}$$

$$= 0.0398 cm^2/s = 3.98 \cdot 10^{-6} m^2/s \tag{S-18}$$

Here a is the radius of the pores inside the catalyst. This is set to 20 nm which is the average pore size for the given catalyst as specified for this support by Saint-Gobain NorPro. The bulk diffusion coefficient is the same as that determined in Eq. S-5.

ϕ_c, ϑ_c, and τ_c have been estimated to the respective values of 0.33, 0.8, and 2.5. Whereby the effective diffusion coefficient can be calculated as:

$$D_e = \frac{0.33 \cdot 0.8}{2.5} \cdot \frac{1}{\frac{1}{3.98 \cdot 10^{-6} m^2/s} + \frac{1}{4.01 \cdot 10^{-9} m^2/s}} \tag{S-19}$$

$$= 4.23 \cdot 10^{-10} m^2/s \tag{S-20}$$

Hereby C_{wp} can be found to be 1.9 and as this criterion states that if $C_{wp} \ll 1$ no interior diffusion problems exist, it is indicated that internal transport limitation probably exist for the largest particles. With a particle size of 300 μm C_{wp} is 0.49.

To further evaluate this, the effectiveness factor (η_{eff}) of a single catalyst pellet was evaluated, which for a first order reaction is given by [1]:

$$\eta_{eff} = \frac{3}{\phi^2} \cdot (\phi \cdot \coth \phi - 1), \tag{S-21}$$

$$\phi^2 = \frac{\rho_c \cdot k_1 \cdot (d_p/2)^2}{D_e} \tag{S-22}$$

In Figure S-2, η_{eff} is plotted as a function of particle size, showing that the smaller particles (radius of 150 μm) has an effectiveness in the order of 97 %, but the larger (radius of 300 μm) are in the order of 89%.

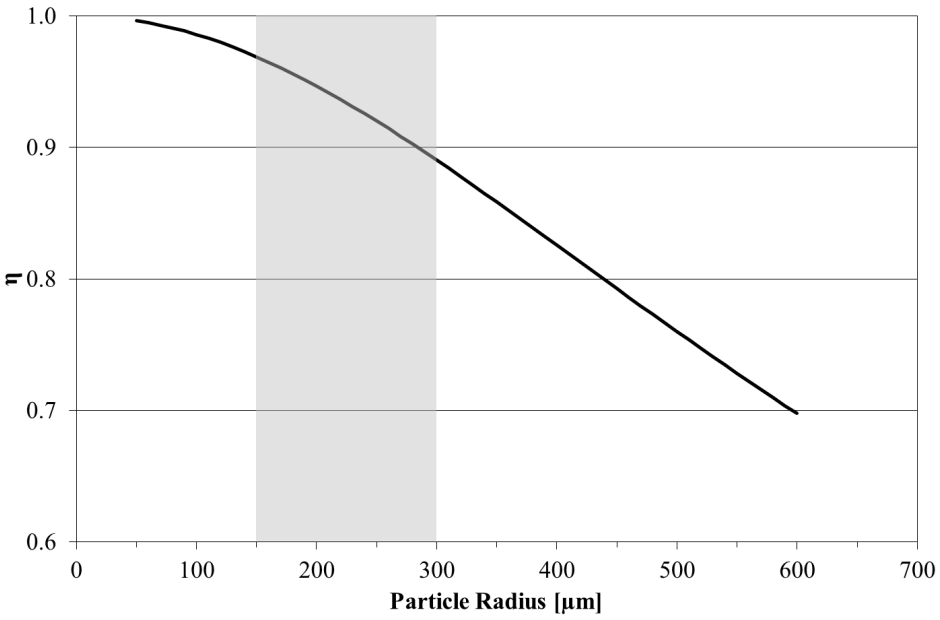

Figure S-2: Effectiveness factor as a function of particle radius for the given system of hydrogenation of guaiacol. Grey area indicate the used particle fraction.

S-3 Kinetic Model Derivation

Based on the experimental observations as summarized in Figure S-3, four main reactions were identified, giving the following kinetic system:

$$r_1 = k_1 \cdot C_{\text{Guaiacol}} \cdot P_{\text{H}_2}^n \tag{S-23}$$

$$r_2 = k_2 \cdot C_{\text{2-Methoxy-cyclohexanol}} \cdot P_{\text{H}_2}^m \tag{S-24}$$

$$r_3 = k_3 \cdot C_{\text{Cyclohexanol}} \cdot P_{\text{H}_2}^l \tag{S-25}$$

$$r_4 = k_4 \cdot C_{\text{1-Octanol}} \cdot P_{\text{H}_2}^k \tag{S-26}$$

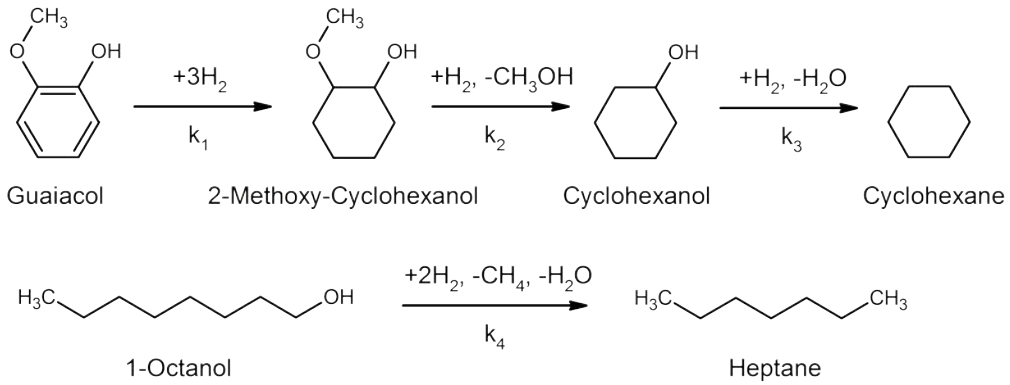

Figure S-3: Observed reaction path of guaiacol and 1-octanol.

Here r_i is the rate of reaction i, k_i is the rate constant for reaction i, C_i is the concentration of compound i, P_{H_2} is the partial pressure of H_2, and n-k are the unknown reaction orders of hydrogen. The reaction orders for all the hydrocarbons were assumed to be quasi first order. Previous work has shown that 1$^{\text{st}}$ order reactions of guaiacol, anisole, and phenol HDO sufficiently describes these systems for simple interpretations [6–8].

As a significant excess of hydrogen was used in all experiments the partial pressure of hydrogen was assumed constant and therefore the kinetic expressions reduce to:

$$r_1 = k_1' \cdot C_{\text{Guaiacol}} \tag{S-27}$$

$$r_2 = k_2' \cdot C_{\text{2-Methoxy-cyclohexanol}} \tag{S-28}$$

$$r_3 = k_3' \cdot C_{\text{Cyclohexanol}} \tag{S-29}$$

$$r_4 = k_4' \cdot C_{\text{1-Octanol}} \tag{S-30}$$

By defining X_1 as the degree of conversion in reaction 1 relative to the initial guaiacol concentration, X_2 as the degree of conversion in reaction 2 relative to the initial guaiacol concentration, X_3 as the degree of conversion in reaction 3 relative to the initial guaiacol concentration, and X_4 as the degree of conversion in reaction 4 relative to the initial 1-octanol concentration and assuming constant volume, the rate equations can be expressed as:

$$r_1 = k_1' \cdot C_{0,\text{Guaiacol}} \cdot (1 - X_1) \tag{S-31}$$

$$r_2 = k_2' \cdot C_{0,\text{Guaiacol}} \cdot (X_1 - X_2) \tag{S-32}$$

$$r_3 = k_3' \cdot C_{0,\text{Guaiacol}} \cdot (X_2 - X_3) \tag{S-33}$$

$$r_4 = k_4' \cdot C_{0,\text{1-Octanol}} \cdot (1 - X_4) \tag{S-34}$$

The reaction takes place in a plug flow reactor, for which the mole balances are [1]:

$$C_{0,\text{Guaiacol}} \cdot v \cdot \frac{dX_1}{dW} = r_1 \tag{S-35}$$

$$C_{0,\text{Guaiacol}} \cdot v \cdot \frac{dX_2}{dW} = r_2 \tag{S-36}$$

$$C_{0,\text{Guaiacol}} \cdot v \cdot \frac{dX_3}{dW} = r_3 \tag{S-37}$$

$$C_{0,\text{1-Octanol}} \cdot v \cdot \frac{dX_4}{dW} = r_4 \tag{S-38}$$

Here v is the feed flow and W is the mass of catalyst. Using zero as initial conditions of the conversions, the differential equation can be solved algebraically as:

$$X_1 = 1 - \exp\left(-k_1' \cdot \frac{W}{v}\right) \tag{S-39}$$

$$X_2 = 1 - \frac{k_1' \cdot \exp\left(-k_2' \cdot \frac{W}{v}\right) - k_2' \cdot \exp\left(-k_1' \cdot \frac{W}{v}\right)}{k_1' - k_2'} \tag{S-40}$$

$$X_3 = 1 - \frac{k_3' \cdot k_2' \cdot \exp\left(-k_1' \cdot \frac{W}{v}\right)}{(k_1' - k_3') \cdot (k_1' - k_2')} \tag{S-41}$$

$$+ \frac{k_3' \cdot k_1' \cdot \exp\left(-k_2' \cdot \frac{W}{v}\right)}{(k_1' - k_2') \cdot (k_2' - k_3')} - \frac{k_1' \cdot k_2' \cdot \exp\left(-k_3' \cdot \frac{W}{v}\right)}{(k_2' - k_3') \cdot (k_1' - k_3')} \tag{S-42}$$

$$X_4 = 1 - \exp\left(-k_4' \cdot \frac{W}{v}\right) \tag{S-43}$$

This can be used to evaluate the kinetic parameters of the sytem, where k_1' corresponds to the rate of hydrogenation, k_2' corresponds to the rate of hydrogenolysis, k_3' corresponds to the rate of hydrodeoxygenation, and k_4' corresponds to the rate of cracking/decarbonylation.

S-4 Detailed Evolution of Product Concentration During Stability Tests with Ni/ZrO_2

All liquid samples were analyzed by GC-MS/FID and detailed product compositions were obtained in all experiments. This is summarized in the following figures. All experiments were conducted at 250 °C and 100 bar, with an oil flow of 0.2 ml/min (WHSV = 4.0 h^{-1}) and gas flow of 400 Nml/min.

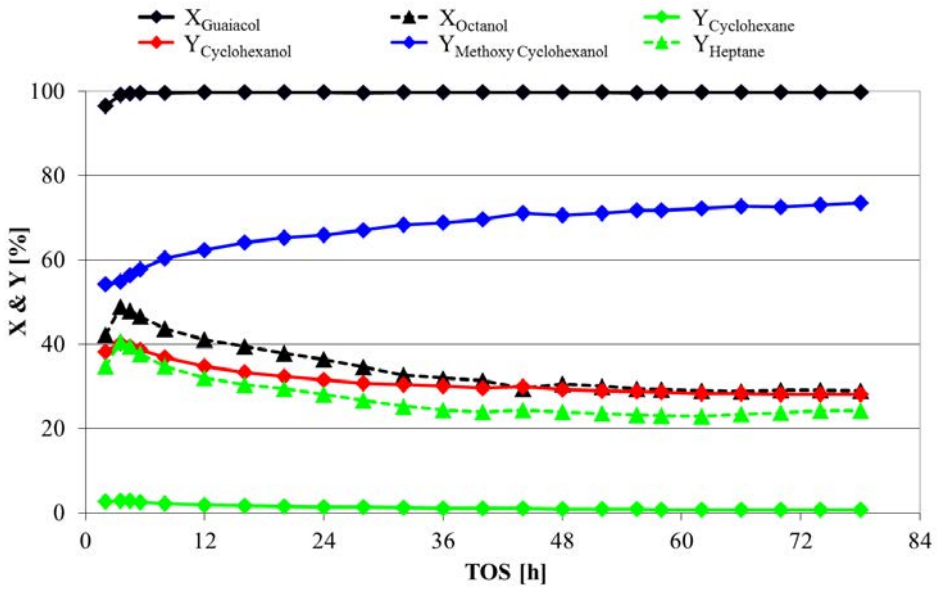

Figure S-4: Conversion of guaiacol and 1-octanol and yield of heptane, cyclohexane, cyclohexanol, 2-methoxy-cylclohexanol DOD for a calcined 5 wt%Ni/ZrO_2 as a function of TOS. T = 250 °C, P = 100 bar, F_{oil} = 0.2 ml/min, WHSV = 4.0 h^{-1}.

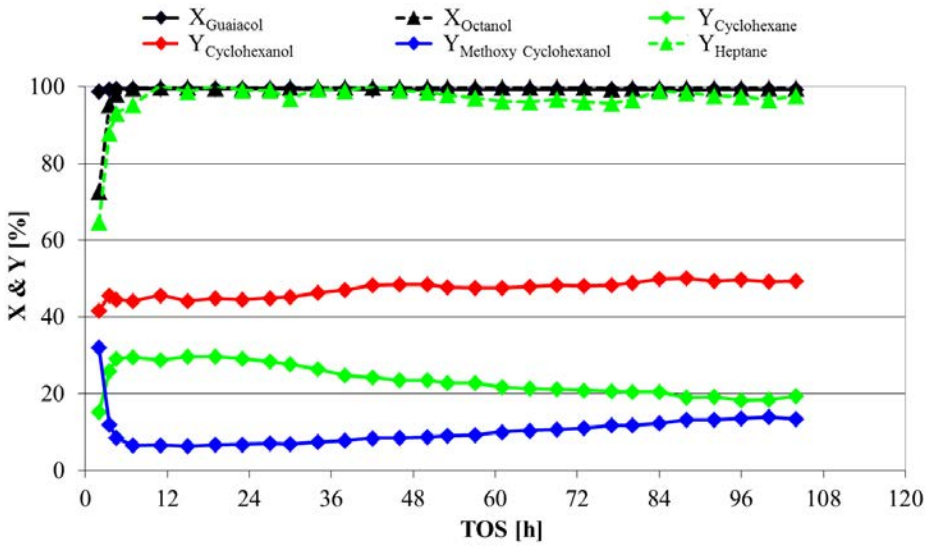

Figure S-5: Conversion of guaiacol and 1-octanol and yield of heptane, cyclohexane, cyclohexanol, 2-methoxy-cylclohexanol DOD for an un-calcined 5 wt%Ni/ZrO_2 as a function of TOS. T = 250 °C, P = 100 bar, F_{oil} = 0.2 ml/min, WHSV = 4.0 h^{-1}.

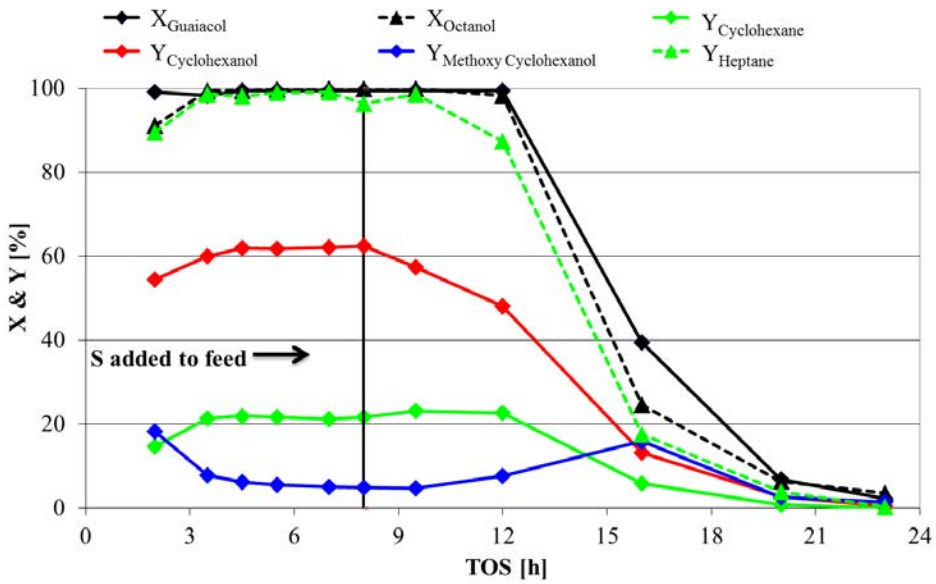

Figure S-6: Conversion of guaiacol and 1-octanol and yield of heptane, cyclohexane, cyclohexanol, 2-methoxy-cylclohexanol DOD for an un-calcined 5 wt%Ni/ZrO_2 as a function of TOS deactivated by 0.05 wt% sulfur from 8 h of TOS. T = 250 °C, P = 100 bar, F_{oil} = 0.2 ml/min, WHSV = 4.0 h^{-1}.

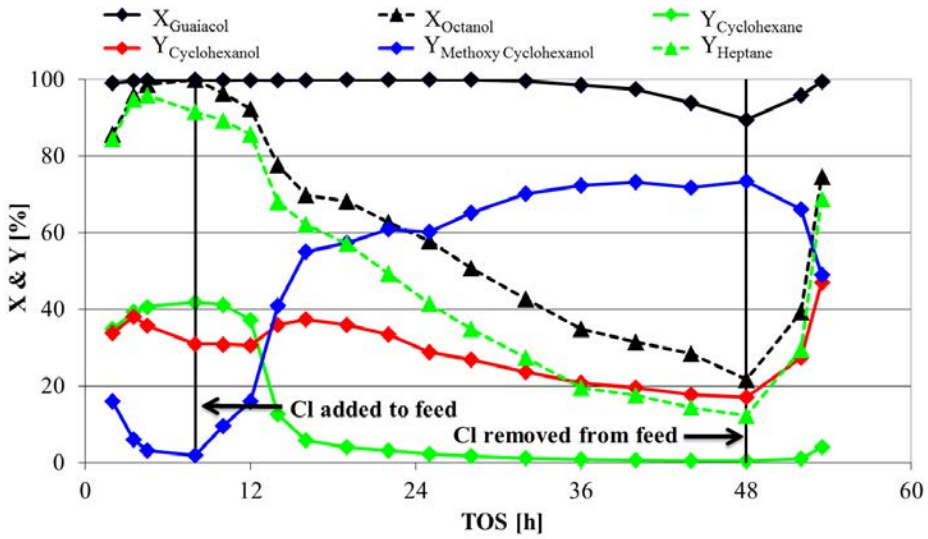

Figure S-7: Conversion of guaiacol and 1-octanol and yield of heptane, cyclohexane, cyclohexanol, 2-methoxy-cylclohexanol DOD for an un-calcined 5 wt%Ni/ZrO_2 as a function of TOS deactivated by 0.05 wt% chlorine from 8 h to 48 h of TOS. T = 250 °C, P = 100 bar, F_{oil} = 0.2 ml/min, WHSV = 4.0 h^{-1}.

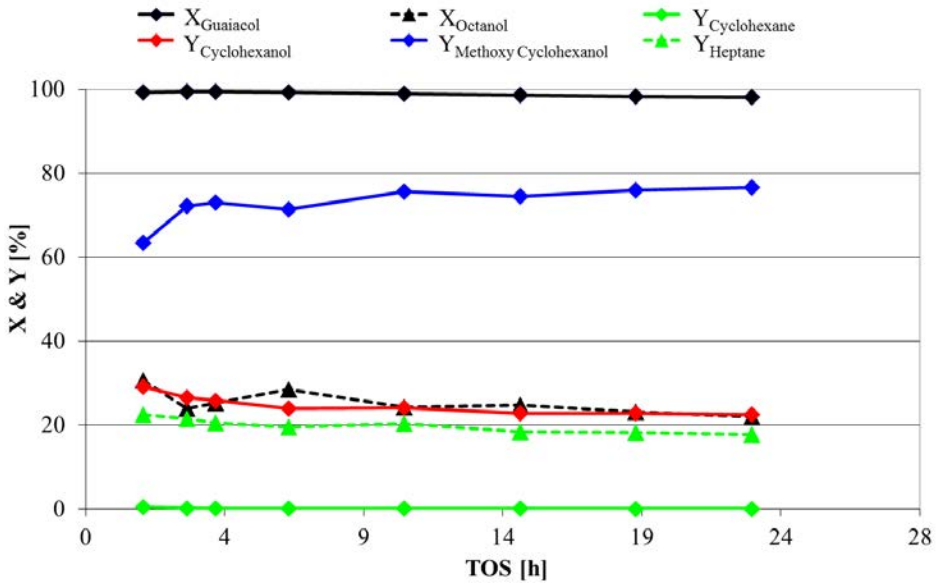

Figure S-8: Conversion of guaiacol and 1-octanol and yield of heptane, cyclohexane, cyclohexanol, 2-methoxy-cylclohexanol DOD for an un-calcined 5 wt%Ni/ZrO_2 impregnated with KCl as a function of TOS. T = 250 °C, P = 100 bar, F_{oil} = 0.2 ml/min, WHSV = 4.0 h^{-1}.

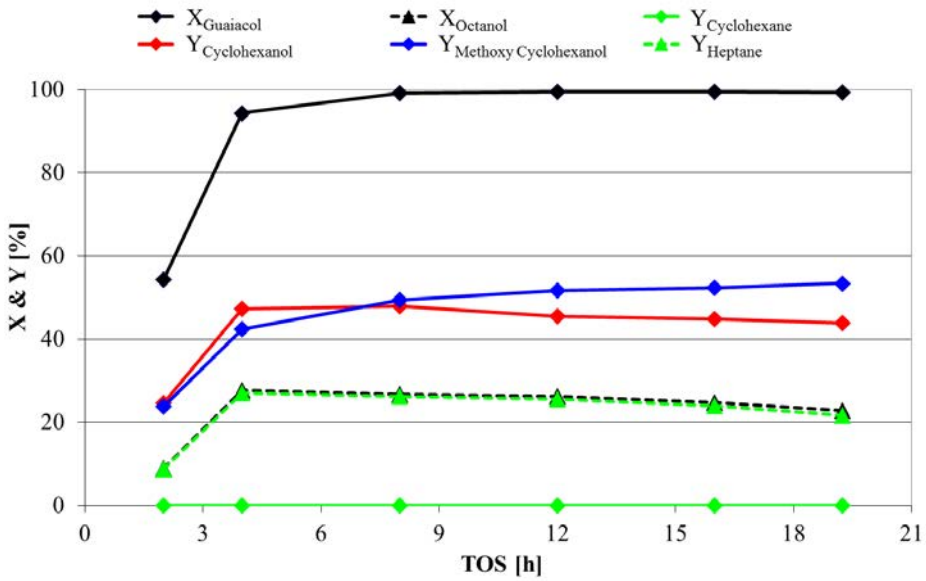

Figure S-9: Conversion of guaiacol and 1-octanol and yield of heptane, cyclohexane, cyclohexanol, 2-methoxy-cylclohexanol DOD for an un-calcined 5 wt%Ni/ZrO_2 impregnated with KNO_3 as a function of TOS. T = 250 °C, P = 100 bar, F_{oil} = 0.2 ml/min, WHSV = 4.0 h^{-1}.

S-5 EXAFS 0Analysi of Poisoned Catalysts

Initially, the local structure of the fresh calcined Ni/ZrO_2 and the in-situ reduction of this catalyst (as discussed in Section S-1) was studied by refining the extended X-ray absorption fine structure (EXAFS) spectra. Figure S-10 presents the experimental and refined Fourier transformed EXAFS spectra (k_3 and k_2 weighted, respectively) of the calcined (Figure 10(a)) and reduced (Figure 10(b)) catalysts. The Fourier transformed spectra, besides being a filter, give an intuitive and immediate idea of the radial atomic distribution around the absorber atom, in this case nickel.

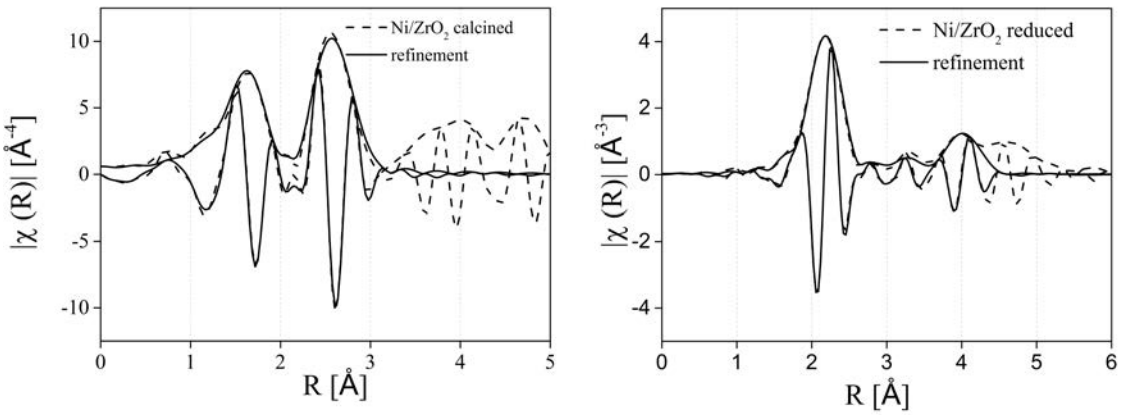

(a) EXAFS of calcined Ni/ZrO_2 (b) EXAFS of reduced Ni/ZrO_2

Figure S-10: Experimental (full line) and refinements (dotted line) Fourier Transformed EXAFS spectra at the Ni-K edge of Ni/ZrO_2 catalysts (a) calcined and (b) reduced (not corrected for phase-shifted).

Due to the shoulder below 2 Å at the Fourier transformed EXAFS spectra (highlighted in Figure B-11(a)), the refinements of carbon, chlorine, KNO_3 and KCl poisoned catalyst were carried out considering one and two shells. The best results were found for the two shells approach. All refinements and Fourier Transformed EXAFS spectra are presented in the figures.

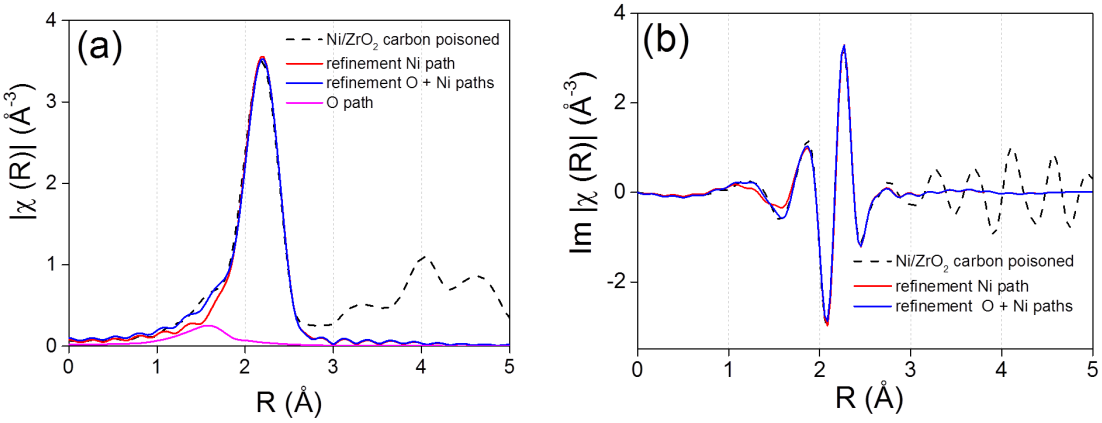

Figure S-11: Fourier transformed EXAFS spectra of carbon poisoned Ni/ZrO_2 catalysts.

Table S-1: Results of the data fits of the Ni-K-edge EXAFS spectra for the carbon poisoned Ni/ZrO_2 catalysts. N is the number of neighboring atoms, r the distance, σ^2 the mean-square disorder in the atomic distances, and ρ the misfit between experimental data and theory. Index f and c respectively indicates fitted and constrained. R-Range: 1.0-3.0 Å, $S_0^2 = 0.78$, 1st model: $\Delta E_0 = 6.6 \pm 0.8$, 2nd: $\Delta E_0 = 5.8 \pm 0.9$

Sample	Model	Atom	N	r [Å]	$\sigma^2 \cdot 10^{-3}$ [Å^2]	ρ [%]
Carbon	1st	Ni	8.6 ± 0.9^f	2.49 ± 0.01^f	6.2 ± 1.0^f	2.6
	2nd	O	0.8 ± 0.3^f	1.98 ± 0.05^f	7.1 ± 0.1^{fa}	0.5
		Ni	8.7 ± 0.9^f	2.48 ± 0.01^f	6.3 ± 1.0^f	

[a] Ni-O σ^2 was constrained and fitted together with $NiCO_3$ reference

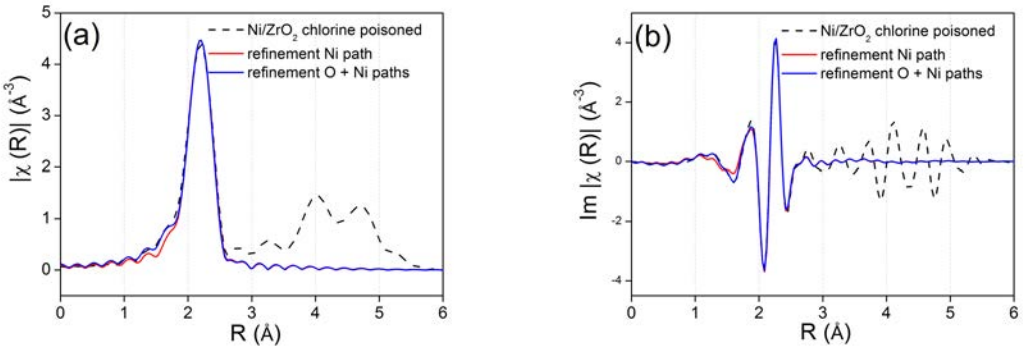

Figure S-12: Fourier transformed EXAFS spectra of chlorine poisoned Ni/ZrO_2 catalysts.

Table S-2: Results of the data fits of the Ni-K-edge EXAFS spectra for the chlorine poisoned Ni/ZrO_2 catalysts. N is the number of neighboring atoms, r the distance, σ^2 the mean-square disorder in the atomic distances, and ρ the misfitt between experimental data and theory. Index f and c respectively indicates fitted and constrained. R-Range: 1.0-3.0 Å, $S_0^2 = 0.78$, 1st model: $\Delta E_0 = 7.0 \pm 0.0$, 2nd model: $\Delta E_0 = 6.6 \pm 1.4$

Sample	Model	Atom	N	r [Å]	$\sigma^2 \cdot 10^{-3}$ [Å^2]	ρ [%]
Chlorine	1st	Ni	8.6 ± 0.8^f	2.49 ± 0.01^f	4.6 ± 1.0^f	1.9
	2nd	O	0.8 ± 0.2^f	2.00 ± 0.04^f	7.2 ± 0.1^{fa}	0.9
		Ni	$8.5 \pm 0.6f$	$2.48^b \pm 0.01^f$	4.5 ± 1.0^f	

[a]Ni-O σ^2 was constrained and fitted together with $NiCO_3$ reference
[b]Fitted uncertainty less than 1%

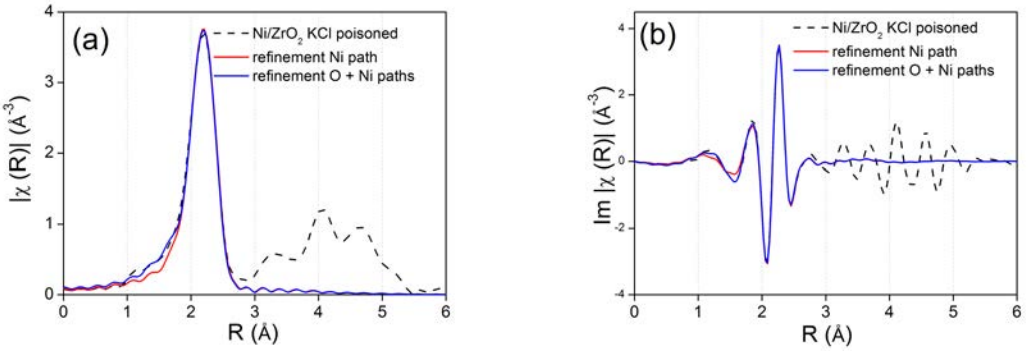

Figure S-13: Fourier transformed EXAFS spectra of KCl poisoned Ni/ZrO_2 catalysts.

Table S-3: Results of the data fits of the Ni-K-edge EXAFS spectra for the KCl poisoned Ni/ZrO_2 catalysts. N is the number of neighboring atoms, r the distance, σ^2 the mean-square disorder in the atomic distances, and ρ the misfit between experimental data and theory. Index f and c respectively indicates fitted and constrained. R-Range: 1.0-3.0 Å, $S_0^2 = 0.78$, 1st model: $\Delta E_0 = 7.1 \pm 0.7$, 2nd model: $\Delta E_0 = 6.7 \pm 0.3$

Sample	Model	Atom	N	r [Å]	$\sigma^2 \cdot 10^{-3}$ [Å^2]	ρ [%]
KCl	1st	Ni	10.0 ± 0.8^f	2.49 ± 0.01^f	7.0 ± 1.0^f	1.2
	2nd	O	0.6 ± 0.1^f	2.00 ± 0.04^f	$7.2 \pm 0.1^{f\,a}$	0.9
		Ni	9.9 ± 0.4^f	$2.48^{f\,b}$	6.8 ± 0.5^f	

[a] Ni-O σ^2 was constrained and fitted together with $NiCO_3$ reference
[b] Fitted uncertainty less than 1%

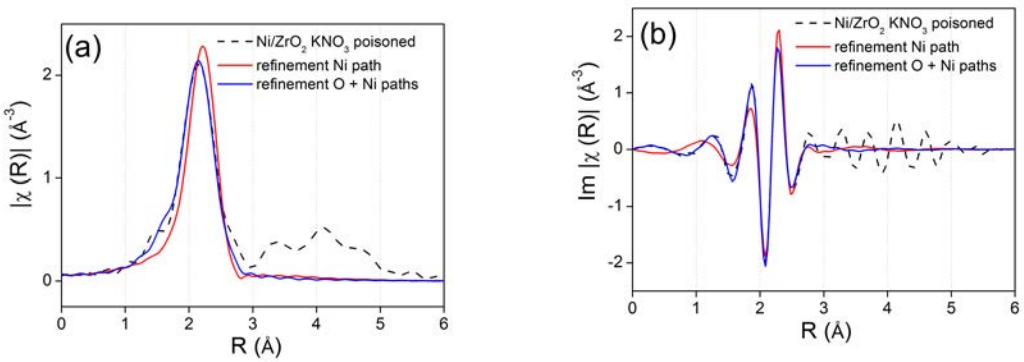

Figure S-14: Fourier transformed EXAFS spectra of KNO_3 poisoned Ni/ZrO_2 catalysts.

Table S-4: Results of the data fits of the Ni-K-edge EXAFS spectra for the KNO_3 poisoned Ni/ZrO_2 catalysts. N is the number of neighboring atoms, r the distance, σ^2 the mean-square disorder in the atomic distances, and ρ the misfit between experimental data and theory. Index f and c respectively indicates fitted and constrained. R-Range: 1.0-3.0 Å, $S_0^2 = 0.78$, 1st model: $\Delta E_0 = 3.3 \pm 2.0$, 2nd model: $\Delta E_0 = 6.6 \pm 1.0$

Sample	Model	Atom	N	r [Å]	$\sigma^2 \cdot 10^{-3}$ [Å^2]	$C_3 \cdot 10^{-4}$ [Å^3]	ρ [%]
KNO_3	1st	Ni	7.5 ± 1.4^f	2.49 ± 0.01^f	8.5 ± 1.6^f	-	5.4
	2nd	O	1.1 ± 0.3^f	1.96 ± 0.01^f	$7.9 \pm 4.5^{f\,a}$		1.3
		Ni	8.3 ± 0.9^f	$2.48 \pm 0.01f$	9.2 ± 1.0^f	$4.9.2 \pm 1.0^f$	

[a] Ni-O σ^2 was constrained and fitted together with $NiCO_3$ reference

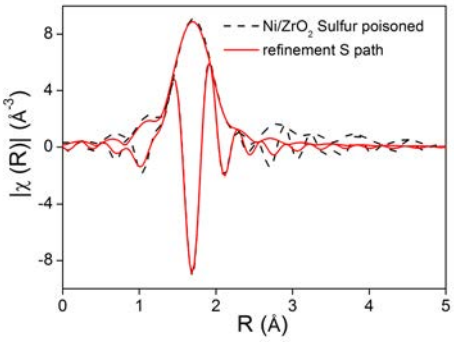

Figure S-15: Fourier transformed EXAFS spectra of sulfur poisoned Ni/ZrO_2 catalysts.

Table S-5: Results of the data fits of the Ni-K-edge EXAFS spectra for the sulfur poisoned Ni/ZrO_2 catalysts. N is the number of neighboring atoms, r the distance, σ^2 the mean-square disorder in the atomic distances, and ρ the misfit between experimental data and theory. Index f and c respectively indicates fitted and constrained. R-Range: 1.11-2.50 Å, $S_0^2 = 0.78$, $\Delta E_0 = -8.4 \pm 0.5$

Sample	Atom	N	r [Å]	$\sigma^2 \cdot 10^{-3}$ [Å^2]	ρ [%]
Suflur	S	5.0^c	2.22 ± 0.01^f	7.6 ± 0.4^f	2.5

References

[1] H. S. Fogler. *Elements of Chemical Reaction Engineering.* Prentice Hall: New Jersey, 2006.

[2] C. R. Wilke and P. Chang. Correlation of diffusion coefficients in dilute solutions. *AIChE J.*, 1:264–270, 1955.

[3] R. B. Bird, W. E. Stewart, and E. N. Lightfoot. *Transport Phenomena.* John Wiley & Sons, Inc.: New York, 2007.

[4] T. Shinomiya. Dielectric dispersion and intermolecular association for 28 pure liquid alcohols the position dependence of hydroxyl group in the hydrocarbon chain. *B. Chem. Soc. Jpn.*, 62:908–914, 1989.

[5] C. N. Satterfield and T. K. Sherwood. *The Role of Diffusion in Catalysis.* Addison-Wesley: London, 1963.

[6] Stephen J. Hurff and Michael T. Klein. Reaction pathway analysis of thermal and catalytic lignin fragmentation by use of model compounds. *Ind. Eng. Chem. Fundam.*, 22:426–430, 1983.

[7] P. M. Mortensen, J.-D. Grunwaldt, P. A. Jensen, and A. D. Jensen. Screening of catalysts for hydrodeoxygenation of phenol as a model compound for bio-oil. *ACS Catal.*, 3:1774–1785, 2013.

[8] M. V. Bykova, S. G. Zavarukhin, L. I. Trusov, and V. A. Yakovlev. Guaiacol hydrodeoxygenation kinetics with catalyst deactivation taken into consideration. *Kinet. Catal.*, 54:40–48, 2013.